energies

MDPI

Article

Dynamic Analysis of a Permanent Magnet DC Motor Using a Buck Converter Controlled by ZAD-FPIC

Fredy E. Hoyos Velasco [1,*], John E. Candelo-Becerra [2] and Alejandro Rincón Santamaría [3]

[1] Escuela de Física, Facultad de Ciencias, Sede Medellín, Universidad Nacional de Colombia, Carrera 65 No. 59A, 110, Medellín 050034, Antioquia, Colombia

[2] Departamento de Energía Eléctrica y Automática, Facultad de Minas, Sede Medellín, Universidad Nacional de Colombia, Carrera 80 No. 65-223, Campus Robledo, Medellín 050041, Antioquia, Colombia; jecandelob@unal.edu.co

[3] Grupo de Investigación en Desarrollos Tecnológicos y Ambientales—GIDTA, Faculty of Engineering and Architecture, Universidad Católica de Manizales, Carrera 23 No. 60-63, Manizales 170002, Caldas, Colombia; arincons@ucm.edu.co

* Correspondence: fehoyosve@unal.edu.co; Tel.: +57-4-4309000 (ext. 46532)

Received: 7 November 2018; Accepted: 30 November 2018; Published: 3 December 2018

Abstract: This paper presents the dynamic analysis of a permanent magnet DC motor using a buck converter controlled by zero average dynamics (ZADs) and fixed-point inducting control (FPIC). Initially, the steady-state behavior of the closed-loop system was observed and then transient behavior analyzed while maintaining a fixed ZAD control parameter and changing the FPIC parameter. Other behaviors were studied when the value of the ZAD control parameter changed and the FPIC parameter was maintained at the initial value. Besides, bifurcation diagrams were built with one and two delay periods by changing the control parameter of the FPIC and maintaining fixed ZAD parameters while some disturbances were carried out in the electric source. The results show that the ZAD-FPIC controller allowed good regulation of the speed for different reference values. The ZAD-FPIC control technique is effective for controlling the buck converter with the motor, even with two delay periods. The robustness of the system was checked by changing the voltage of the source. It was shown that the system used a fixed switching frequency because the duty cycle was not saturated for certain ranges of the control parameters shown in the research. This technique can be used for higher order systems with experimental phenomena such as quantization effects, time delays, and variations in the input signal.

Keywords: buck converter; DC motor; bifurcations in control parameter; sliding control; zero average dynamics; fixed-point inducting control

1. Introduction

Electric motors are designed to perform tasks with high accuracy when completing repetitive tasks [1]. The speed control helps maintain the frequency close to the reference value and allows the motor to offer continuous stability. Recent advances in materials for permanent magnets mean they are now lighter, less expensive, and easier to control at low speed, thus expanding their domestic and industrial applications [2]. Currently in the industry, digital signal processing (DSP) offers the following characteristics: greater versatility compared with analog designs [3]; ease of implementation for nonlinear controllers and advanced control techniques; low-power consumption; reduction of external passive components; low sensitivity to parameter variation; applications of high-frequency switching controllers; and others that have been described in References [4–8]. However, dynamic analyses must be performed to understand the optimal functioning of the controller with loads and the different actions to apply.

The control of motors have been studied previously using zero average dynamics (ZADs) and fixed-point induced control (FPIC) [8]. The FPIC control technique has been used to control chaotic systems applied to DC–DC and DC–AC converters. The time-delay autosynchronization (TDAS) control strategy has shown better convergence results and easy implementation of the digital modulation of centered pulse width (DPWMC). As an alternative, a sliding surface has been used to apply the ZAD control technique in a quasi-sliding manner [9]. Besides, ZAD was used to implement a buck inverter in a field-programmable gate array (FPGA), verifying that the ZAD technique with pulse next meets the requirements of a fixed switching frequency [10,11]. Other studies using the ZAD control strategy have considered the transition from periodic bands to chaotic bands in a buck DC–DC converter. This is useful to identify bifurcations by double period and by corner impact, known as "corner collision bifurcations", as well as chaotic phenomena, chaotic bands, and doubling of these bands [12–14].

The existence of bifurcations and chaos bands for a buck converter operated with DPWMC with and without a delay period controlled with ZAD was analyzed numerically [15]. The dynamic behavior of these systems has been also extensively studied through mathematical, numerical, and experimental analyses [16–18]. In Reference [19], the simulation of a buck converter configured as an inverter was carried out by using the Powersim (PSIM) simulation software professional version 6.1.3 and applying the ZAD technique with PWMC and FPIC. The reference signals to be followed were triangular and sinusoidal, and it was tested for various types of load (i.e., resistive, time-variable, nonlinear, and open-circuit operation).

In Reference [20], a quasi-sliding algorithm based on ZAD was proposed for the modular control of the DC–AC conversion system by connecting m single-phase inverters in parallel to feed the same load. In Reference [21], numerical and experimental results were obtained by applying digital control implemented in a DSP using the ZAD-FPIC control technique to a DC–DC and a DC–AC converter. It was shown that the bifurcation diagrams, calculated numerically in the design stage, agree quantitatively with those obtained in the experimental stage.

The integration of ZAD with an FPIC controller has been shown to work well for the buck converter, regulating resistive and motor loads [8]. However, the dynamics of the control connected to the motors must be studied. Therefore, this paper focuses on the dynamic analysis of a buck converter that uses the combined ZAD-FPIC control technique to control the speed of an electric motor. The system involves a buck power converter, a permanent magnet DC motor, and a dSPACE platform [22]. The load torque and the friction torque were considered as known. The ZAD-FPIC scheme was formulated and experimentally tested. Bifurcation diagrams were developed for the adaptive ZAD-FPIC control system for different values of the controller parameters. The tests performed in the research show how the numerical and experimental diagrams match for the initial conditions and the changes carried out in the study. The main differences of the present paper with respect to closely related papers on ZAD-FPIC [23,24] are the following: the ZAD-FPIC technique was proven for the first time in a higher order system (a permanent magnet DC motor). In previous works, the ZAD-FPIC technique was only applied to second-order systems and no analysis related to bifurcation for the FPIC technique has been performed [8]. In this work, some disturbance in the input voltage and the control with one and two delay periods have been applied, achieving effectiveness in speed control. It was proved that the FPIC technique is useful to control the chaos and to follow the speed to a reference given by the user.

This paper is organized as follows. Section 2 presents the materials and methods used in the research and the mathematics required to perform the simulation and experimental tests. Section 3 includes the results and analysis of the different simulation and experimental tests performed with the proposed changes in the control parameters and the reference source. Section 4 presents the conclusions of the work.

2. Materials and Methods

Figure 1 shows the block diagram of the system under study that considers a motor connected to a buck converter and controlled by the ZAD-FPIC technique, and referred to in this research as the "buck-motor system". Some sensors are used to measure the voltage, current, and speed of the buck-motor system. The controller considers these signals, and with the reference speed, takes actions on the buck converter to regulate the speed of the DC motor. In this research, the speed reference and the control parameters are varied in order to identify how the controller regulates the speed of the motor.

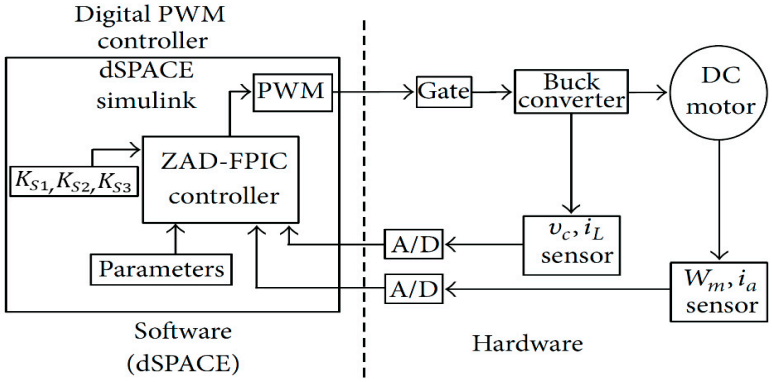

Figure 1. Buck converter connected to an electric DC motor and controlled by zero average dynamics-fixed-point induced control (ZAD-FPIC).

The system presented in Figure 1 considers a permanent magnet motor with the following characteristics as presented in Table 1.

Table 1. Rated values of the DC motor.

Parameter	Description	Value
P_r	Rated power	250 W
V_r	Rated voltage	42 VDC
I_r	Rated current	6 A
W_r	Rated speed	4000 RPM

The speed of the motor is measured by using an encoder of 1000 pulses per revolution. The state variables, established as the output voltage v_c, the inductor current i_L, and armature current i_a, are measured with an accurate resistance. The digital communication was performed by using a board with DS1104 of dSPACE, where the techniques of ZAD-FPIC are implemented. The output PWM is calculated by a DS1104 that sends the digital signal. The connection of the control system with the power system is performed with opto-couplers with fast response, such as HCPL-J312, which protect and isolate the digital circuit from possible currents and voltages generated in the power circuit. The state variables, v_c, i_L, and i_a, reach the controller based on the input ADC of 12 bits. The controlled variable W_m is measured by an encoder of 28 bits at sample frequencies of 6 kHz.

The parameters related to the DC electric motor parameters, buck converter, and law of ZAD-FPIC control are defined in the control blocks. The last parameters are related to the time constants and the dynamics of the error that is to be imposed in the control system, for example, K_{S1}, K_{S2}, and K_{S3}. At each sampling period, the microprocessor of the DS1104 calculates, with a resolution of 10 bits, the duty cycle d and its equivalent to the PWMC to control the solid-state switch S (metal-oxide-semiconductor field-effect transistor or MOSFET).

2.1. Model of the Buck Motor System

Equations (1) and (2) represent the DC motor and the mechanical load. This model considers a second order, where the state variables are the speed of the motor W_m (rad/s) and the armature current i_a (A). The term k_e represents the constant of the output voltage in the motor (V/rad/s), L_a is the armature inductance (mH), R_a is the armature resistance (Ω), $V_a = v_c$ is the voltage in the motor (V), B is the viscosity friction coefficient (N·m/rad/s), J_{eq} is the inertia moment (kg·m^2), k_t is the torque constant of the motor (N·m/A), T_{fric} is the friction torque (N·m), T_L is the load torque (N·m), and J_L is the moment of inertia of the load (kg·m^2):

$$\frac{dW_m(t)}{dt} = \frac{-BW_m(t)}{J_{eq}} + \frac{k_t i_a(t)}{J_{eq}} + \frac{-T_{fric}}{J_{eq}} + \frac{-T_L}{J_{eq}}, \tag{1}$$

$$\frac{di_a(t)}{dt} = \frac{-k_e}{L_a} W_m(t) + \frac{-R_a}{L_a} i_a(t) + \frac{v_c}{L_a}. \tag{2}$$

To model the buck-motor system and obtain a representation in state variables, the system of Figure 2 is analyzed. This figure shows that the equivalent diagram depends on the state of the switch S. For this system, the speed of the motor can be changed by manipulating the switch ON and OFF by changing the model as described next. The parameters of the buck-motor system are shown in Table 2.

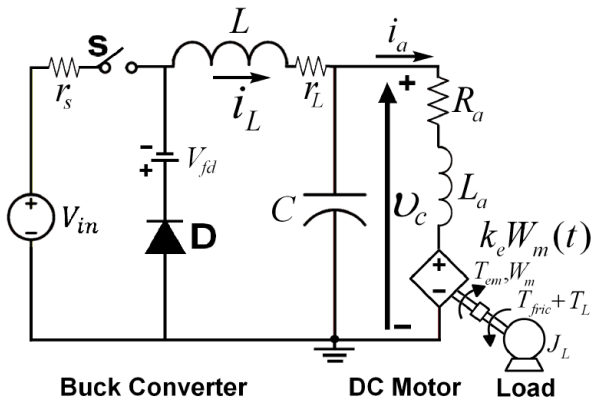

Figure 2. Diagram of the buck converter connected to a DC motor.

Table 2. Parameters of the buck-motor system.

Parameter	Description	Value
r_s	Internal resistance of the source	0.84 Ω
V_{in}	Input voltage	40.086 V
V_{fd}	Diode forward voltage	1.1 V
L	Inductance	2.473 mH
r_L	Internal resistance of the inductor	1.695 Ω
C	Capacitance	46.27 µF
R_a	Armature resistance	2.7289 Ω
L_a	Armature inductance	1.17 mH
B	Viscosity friction coefficient	0.000138 (N·m/rad/s)
J_{eq}	Inertia moment	0.000115 (kg·m^2)
k_t	Motor torque constant	0.0663 (N·m/A)
k_e	Voltage constant	0.0663 (V/rad/s)
T_{fric}	Friction torque	0.0284 (N·m)
T_L	Load torque	Variable (N·m)
W_m	Speed of the motor [rad/s]	28 bits
i_a	Armature current [A]	12 bits
v_c	Voltage of the motor [V]	12 bits
i_L	Current in the inductor [A]	12 bits

Figure 3 illustrates the operation in continuous driving mode with the switch closed (S = ON) and the diode in cut (inactive). This circuit considers the main source E, the parasite resistance $r_s = r_{s1} + r_M$ as the sum of the internal resistance of the source r_{s1} and the parasite resistance of the MOSFET r_M, the inductance L, and the capacitance C. The load is a DC motor that considers the armature resistance R_a and armature inductance L_a.

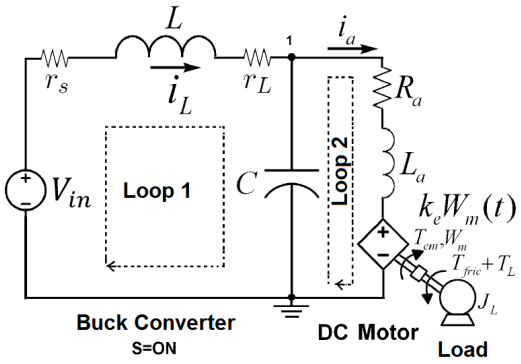

Figure 3. Electromechanical system with the switch ON.

Applying the Kirchhoff laws to the circuit in Figure 3, the mathematical model of this new equivalent circuit can be represented as in Equation (3). In a simple form, this expression can be presented as $\dot{x} = A_1 x + B_1$, where $x_1 = W_m$, $x_2 = i_a$, $x_3 = v_c$, and $x_4 = i_L$:

$$\begin{bmatrix} \dot{W}_m \\ \dot{i}_a \\ \dot{v}_c \\ \dot{i}_L \end{bmatrix} = \begin{bmatrix} \frac{-B}{J_{eq}} & \frac{k_t}{J_{eq}} & 0 & 0 \\ \frac{-k_e}{L_a} & \frac{-R_a}{L_a} & \frac{1}{L_a} & 0 \\ 0 & \frac{-1}{C} & 0 & \frac{1}{C} \\ 0 & 0 & \frac{-1}{L} & \frac{-(r_L+r_s)}{L} \end{bmatrix} \begin{bmatrix} W_m \\ i_a \\ v_c \\ i_L \end{bmatrix} + \begin{bmatrix} \frac{-(T_{fric}+T_L}{J_{eq}} \\ 0 \\ 0 \\ \frac{V_{in}}{L} \end{bmatrix}. \quad (3)$$

On the other hand, Figure 4 shows the diagram of the circuit with the diode in conduction mode and the switch open (S = OFF). Thus, the initial circuit is reduced to an equivalent circuit as that presented in Figure 4.

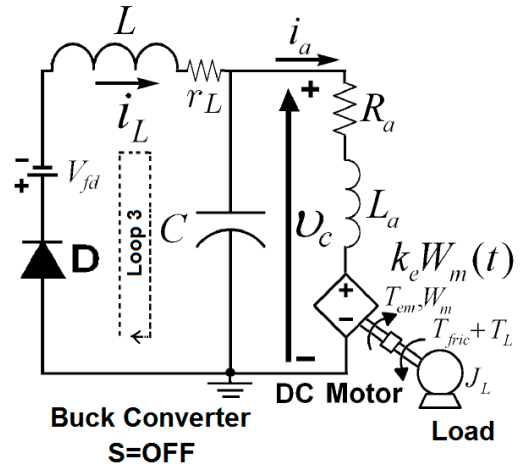

Figure 4. Electromechanical system with the switch OFF.

In this case, the mathematical model of this new equivalent circuit can be represented as Equation (4), what in a simple form can be presented as $\dot{x} = A_2 x + B_2$. The state variables are W_m, i_a, v_c, and i_L, and the parameters C and L are the capacitance and inductance of the converter, respectively. The parasite resistance $r_s = r_{s1} + r_M$ is equal to the sum of the internal resistance of the

source and the parasite resistance of the MOSFET. The resistance $r_L = r_{L1} + r_{Med}$ is equal to the sum of the resistances of the winding and the current measurement, and V_{fd} is the voltage in the direct conduction diode. The source that feeds the buck-motor system is represented by the input voltage V_{in} and depends on the switch S controlled by the pulses of the PWMC; that is, the system feeds with V_{in} when S is active, or with $-V_{fd}$ when S is inactive:

$$\begin{bmatrix} \dot{W}_m \\ \dot{i}_a \\ \dot{v}_c \\ \dot{i}_L \end{bmatrix} = \begin{bmatrix} \frac{-B}{J_{eq}} & \frac{k_t}{J_{eq}} & 0 & 0 \\ \frac{-k_e}{L_a} & \frac{-R_a}{L_a} & \frac{1}{L_a} & 0 \\ 0 & \frac{-1}{C} & 0 & \frac{1}{C} \\ 0 & 0 & \frac{-1}{L} & \frac{-(r_L)}{L} \end{bmatrix} \begin{bmatrix} W_m \\ i_a \\ v_c \\ i_L \end{bmatrix} + \begin{bmatrix} \frac{-(T_{fric}+T_L}{J_{eq}} \\ 0 \\ 0 \\ \frac{-V_{fd}}{L} \end{bmatrix}. \quad (4)$$

The buck-motor system can present a discontinuous conduction mode (DCM) when the switch is open and the currents in the inductor are zero. In this case, the diode stops conducting and the circuit can be represented as shown in Figure 5, with the differential equations shown in Equation (5). This last equation can be rewritten as $\dot{x} = A_{\text{DCM}}x + B_{\text{DCM}}$.

$$\begin{bmatrix} \dot{W}_m \\ \dot{i}_a \\ \dot{v}_c \\ \dot{i}_L \end{bmatrix} = \begin{bmatrix} \frac{-B}{J_{eq}} & \frac{k_t}{J_{eq}} & 0 & 0 \\ \frac{-k_e}{L_a} & \frac{-R_a}{L_a} & \frac{1}{L_a} & 0 \\ 0 & \frac{-1}{C} & 0 & 0 \\ 0 & 0 & 0 & 0 \end{bmatrix} \begin{bmatrix} W_m \\ i_a \\ v_c \\ i_L \end{bmatrix} + \begin{bmatrix} \frac{-(T_{fric}+T_L)}{J_{eq}} \\ 0 \\ 0 \\ 0 \end{bmatrix}. \quad (5)$$

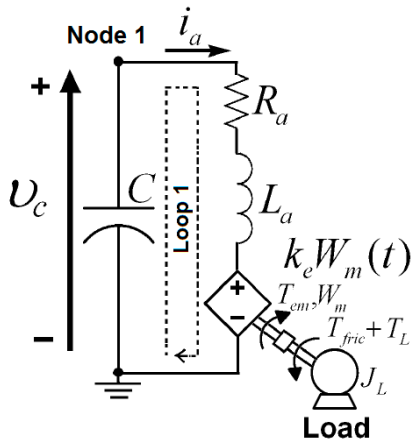

Figure 5. Buck-motor system working in discontinuous conduction mode (DCM).

Assuming that the PWM signal is configured with the pulse to the center and the buck-motor system works in continuous conduction mode (CCM), the dynamics of the system in a complete period are described by Equation (1) and can be written as:

$$\dot{x} = \begin{cases} A_1 x + B_1 & \text{if} \quad kT \le t \le kT + dT/2 \\ A_2 x + B_2 & \text{if} \quad kT + dT/2 < t < kT + T - dT/2 \\ A_1 x + B_1 & \text{if} \quad kT + T - dT/2 < t < kT + T \end{cases}. \quad (6)$$

The term k represents the k-th iteration of the system with one sample period T or commutation period. The derivate of the state is defined as $\dot{x}$ and can be calculated as shown in Equation (7):

$$\dot{x} = \left[\dot{x}_1, \dot{x}_2, \dot{x}_3, \dot{x}_4\right]^T \equiv \left[\frac{dx_1}{dt}, \frac{dx_2}{dt}, \frac{dx_3}{dt}, \frac{dx_4}{dt}\right]^T \equiv \left[\frac{dW_m}{dt}, \frac{di_a}{dt}, \frac{dv_c}{dt}, \frac{di_L}{dt}\right]^T. \quad (7)$$

2.2. Analytical Solution of the Buck-Motor System

In this work, the system is assumed to operate in the CCM. The solution of the system equations presented in Equation (6) is obtained as shown in Equation (8):

$$x(t) = \begin{cases} e^{A_1 t} M_1 - V_1 & \text{if} \quad kT \leq t \leq (k + d/2)T \\ e^{A_2 t} M_2 - V_2 & \text{if} \quad (k + d/2)T < t < (k + 1 - d/2\,)T \\ e^{A_1 t} M_3 - V_1 & \text{if} \quad (k + 1 - d/2\,)T \leq t \leq (k+1)T \end{cases}, \tag{8}$$

where

$$\begin{aligned} M_1 &= x(0) + V_1 \\ M_2 &= Q_{12} M_1 - \Delta V e^{-A_2 T \frac{d}{2}} \\ M_3 &= Q_{21} M_2 + \Delta V e^{-A_1 T (1 - \frac{d}{2})} \\ Q_{12} &= e^{(A_1 - A_2) T (\frac{d}{2})} \\ Q_{21} &= e^{(A_2 - A_1) T (1 - \frac{d}{2})} \\ V_1 &= A_1^{-1} B_1 \\ V_2 &= A_2^{-1} B_2 \\ \Delta V &= V_1 - V_2 \end{aligned}$$

The solution when the system operates in DCM is given by Equation (9) and is presented when the current in the inductor is zero:

$$x(t) = e^{A_{\text{DCM}} t} \left[x(0) + A_{\text{DCM}}^{-1} B_{\text{DCM}} \right] - A_{\text{DCM}}^{-1} B_{\text{DCM}}. \tag{9}$$

Starting from the solution in Equation (8) and discretizing the output signals for each sampling period T, we have the expression in discrete time given by Equation (10), which is the solution in CCM for the buck-motor system:

$$x((k+1)T) = e^{A_1 T} Q x(kT) + e^{A_1 T} Q V_1 - Q_{12} e^{A_2 T (1 - \frac{d}{2})} \Delta V + e^{A_1 T \frac{d}{2}} \Delta V - V_1. \tag{10}$$

The term Q is obtained with Equation (11) and the expressions are defined in Equations (5) and (6):

$$Q = e^{(A_2 - A_1) T} e^{(A_1 - A_2) T d}. \tag{11}$$

The solution of the system operating in DCM is given in Equation (12):

$$x((k+1)T) = e^{A_{\text{DCM}} T} \left[x(kT) + A_{\text{DCM}}^{-1} B_{\text{DCM}} \right] - A_{\text{DCM}}^{-1} B_{\text{DCM}}. \tag{12}$$

2.3. Strategies to Control the Speed of the DC Motor

The speed W_m of the DC motor must follow a reference speed W_{mref}. Thus, for the sampling period kT, the tracking error is defined as presented in Equation (13):

$$e(kT) = W_m(kT) - W_{mref}(kT). \tag{13}$$

Besides, considering the system in fourth-order, the sliding surface is defined as $s(kT)$ [20], describing a third-order dynamic in the error variable ($e(kT)$), which is given by Equation (14):

$$s(kT) = e(kT) + k_{s1} \frac{de(kT)}{d(kT)} + k_{s2} \frac{d^2 e(kT)}{d(kT)^2} + k_{s3} \frac{d^3 e(kT)}{d(kT)^3}. \tag{14}$$

The constants $k_{s1} = K_{S1}\sqrt{LC}$, $k_{s2} = K_{S2} LC$, and $k_{s3} = K_{S3} LC \sqrt{LC}$ are parameterized in function of the constants applied (K_{S1}, K_{S2}, and K_{S3}). The constants K_{S1}, K_{S2}, and K_{S3} are the parameters of

the ZAD and can be calibrated to impose a dynamic behavior in the closed-loop system. In addition, such parameters can be considered to construct dimensional bifurcation diagrams. When the reference signal W_{mref} is established as a constant value, Equation (14) can be written as in Equation (15) and the first derivate as in Equation (16):

$$s(kT) = W_m(kT) - W_{mref}(kT) + k_{s1}\frac{dW_m(kT)}{d(kT)} + k_{s2}\frac{d^2W_m(kT)}{d(kT)^2} + k_{s3}\frac{d^3W_m(kT)}{d(kT)^3}\ , \tag{15}$$

$$\dot{s}(kT) = \frac{dW_m(kT)}{d(kT)} + k_{s1}\frac{d^2W_m(kT)}{d(kT)^2} + k_{s2}\frac{d^3W_m(kT)}{d(kT)^3} + k_{s3}\frac{d^4W_m(kT)}{d(kT)^4}. \tag{16}$$

The duty cycle can be calculated as shown in Equation (17):

$$d_k(kT) = \frac{2s(kT) + T\dot{s}_-(kT)}{T\left(\dot{s}_-(kT) - \dot{s}_+(kT)\right)}, \text{is} \tag{17}$$

where $s(kT)$ is calculated as shown in Equation (15) at the beginning of each commutation period for the system in Equation (3). Thus, $s(kT) = s(kT)|_{\ S=ON}$; $\dot{s}_+(kT)$ is calculated as in Equation (16) for the system described in Equation (3) as $\dot{s}_+(kT) = \dot{s}(kT)|_{\ S=ON}$ [8].

Next, the necessary steps to calculate the variables are: the first derivatives taken from the system are obtained from Equation (3), which occurs when $S =$ ON. To obtain $\dot{s}_-(kT)$, the first, second, third, and fourth derivates are calculated for the system and $\dot{s}_-(kT) = \dot{s}(kT)|_{\ S=OFF}$. With the delay period in the control action, the new duty cycle is calculated as in Equation (18):

$$d_k(kT) = \frac{2s((k-1)T) + T\dot{s}_-((k-1)T)}{T\left(\dot{s}_-((k-1)T) - \dot{s}_+((k-1)T)\right)}. \tag{18}$$

With the ZAD-FPIC strategy, the new duty cycle is calculated to ensure that the load and the motor rotate at the desired speed W_{mref}, leading to the expression shown in Equation (19):

$$d_{\text{ZAD}-\text{FPIC}}(kT) = \frac{d_k(kT) + Nd^*}{N+1}. \tag{19}$$

Combining Equations (18) and (19), the control for the ZAD-FPIC is defined as in Equation (20):

$$d_{\text{ZAD}-\text{FPIC}}(kT) = \left(\frac{2s((k-1)T) + T\dot{s}_-((k-1)T)}{T\left(\dot{s}_-((k-1)T) - \dot{s}_+((k-1)T)\right)} + Nd^*\right)(N+1)^{-1}. \tag{20}$$

where d^* is calculated at the beginning of the period with

$$d^* = d_k(kT)|_{\ stable\ state}. \tag{21}$$

Therefore, Equation (20) combines ZAD and FPIC techniques, and a saturation function must be applied to consider the actual physical limits of the duty cycle between 0 and 1. Such a saturation function is described in Equation (22):

$$d = \begin{cases} d_{\text{ZAD}-\text{FPIC}}(kT) \text{ if } 0 < d_{\text{ZAD}-\text{FPIC}}(kT) < 1 \\ 1 \text{ if } 1 \leq d_{\text{ZAD}-\text{FPIC}}(kT) \\ 0 \text{ if } d_{\text{ZAD}-\text{FPIC}}(kT) \leq 0 \end{cases}. \tag{22}$$

3. Results and Analysis

This section presents the results obtained from the dynamic analysis of a DC motor using a buck converter controlled by ZAD-FPIC. The quantization effects considered in the tests are: 28 bits of speed, 12 bits in the system variables (v_c, i_a, and i_L), and 10 bits for the duty cycle. MATLAB®/Simulink

software was used for the simulation, and the simulation blocks that represent the system with ZAD-FPIC controller are shown in Figure 6. For the experimental test, the ZAD-FPIC technique is implemented in the rapid control prototyping card dSPACE DS1104; in this case, the card is programmed with MATLAB®/Simulink and then downloaded to the DSP. This platform has a graphical display interface called ControlDesk. In order to overlap the numerical with the experimental results, the experimental data were stored in matrices using the ControlDesk program and then read to perform calculations in MATLAB. Finally, the simulation is run and both the numerical and experimental results plotted.

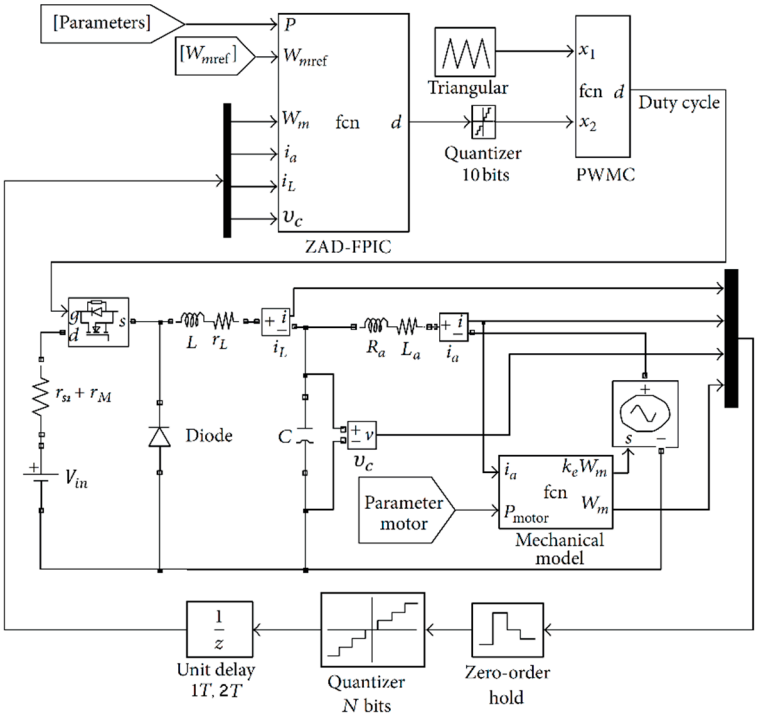

Figure 6. ZAD-FPIC controller simulation blocks.

3.1. Parameters of the Controller

Table 3 shows the parameters of the ZAD-FPIC controller used in the simulation and experimental tests.

Table 3. Parameters of the ZAD-FPIC controller.

Parameter	Description	Value
V_{in}	Input voltage	40.086 V
W_{mref}	Reference speed	Variable (rad/s)
N	Control parameter of FPIC	1
Fc	Commutation frequency	6 kHz
Fs	Sample frequency	6 kHz
$1T\_p$	1 delay period	166.6 µs
K_{S1}, K_{S2}, K_{S3}	Bifurcation parameter	Variables
d	Duty cycle	10 bits

3.2. Behavior of the Buck-Motor System in Closed Loops

Figure 7 shows the dynamic behavior of the mechanical speed and the error of the signals when the electric circuit works in closed loops. The speed is determined for both simulation and experimental tests following a change in the reference signal W_{mref}. Figure 7a,b show the mechanical speed and

the error over time, respectively, when the circuit works in a closed loop. In this case, the system is working in a closed loop when the reference signal is W_{mref} = 400 rad/s at t = 1 s, K_{S1} = 2, K_{S2} = 2, K_{S3} = 30, and N = 1 with one delay period.

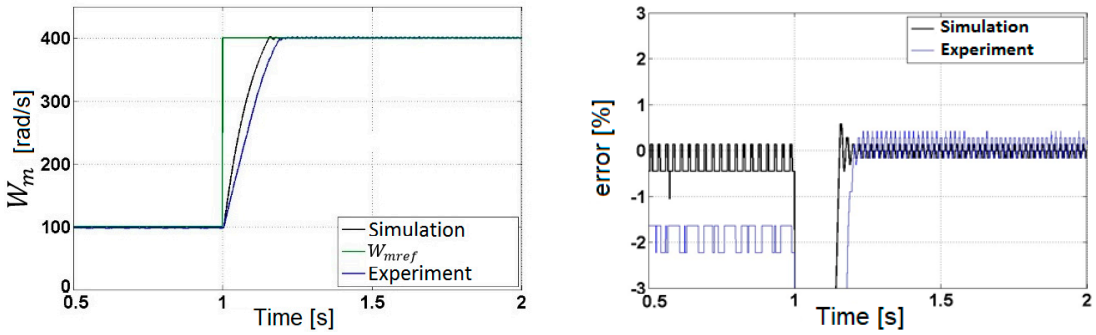

Figure 7. Numerical and experimental results for the system in closed loops: (**a**) mechanical speed W_m and W_{mref} in closed loop and (**b**) error of W_m in closed loop.

Figure 7a shows that the impulse is very small for the simulation and experimental tests; the settling time of W_m is t_s = 0.1473 s in the simulation test and t_s = 0.1859 s in the experimental test. Finally, Figure 7b shows that the steady-state error in the simulation test is −0.1645% and for the experimental test it is 0.4245%.

Table 4 summarizes the simulated and experimental results for the closed-loop systems shown in Figure 7.

Table 4. Transient responses of the buck-motor system in closed-loop with ZAD-FPIC.

Controller	M_p (%)	t_s (s)	Error (%)
Closed-loop system in the simulation test	0.5715	0.1473	−0.1645
Closed-loop system in the experimental test	Overdamped	0.1859	0.4245

Figure 8 shows the behavior of the system working closed loops for the simulation and experimental test when the reference signal W_{mref} changes from 100 to 400 rad/s in intervals of 4 s. In the experimental test, the closed-loop system did not present an impulse, whereas for the simulation test, some small impulses are presented for the closed-loop system. The signals (W_m) present a settling time of $t_s \cong 0.15$ s. The steady-state error for the closed-loop system is less than 2%. There is a high coincidence between the numerical and experimental results. From the results shown in Figure 8a,b, the ZAD-FPIC controller is robust to the variations created in the reference signal.

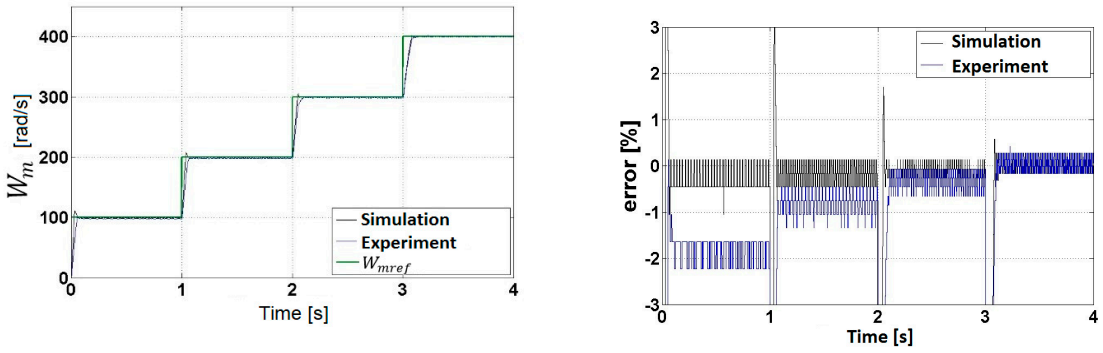

Figure 8. Numerical and experimental results in closed loops: (**a**) mechanical speed W_m and reference speed W_{mref} in a closed-loop system and (**b**) error of W_m in a closed-loop system.

3.3. Transient Response Changing the Control Parameter N with Parameter K_{S3} = 35

Figure 9 shows the behavior of the buck-motor system controlled by ZAD-FPIC. In this case, the control parameter is fixed as $K_{S3} = 35$, the reference signal is defined as $W_{mref} = 400$ rad/s, and some variations are made through the control parameter N in values 1, 3, 5, 7, and 9.

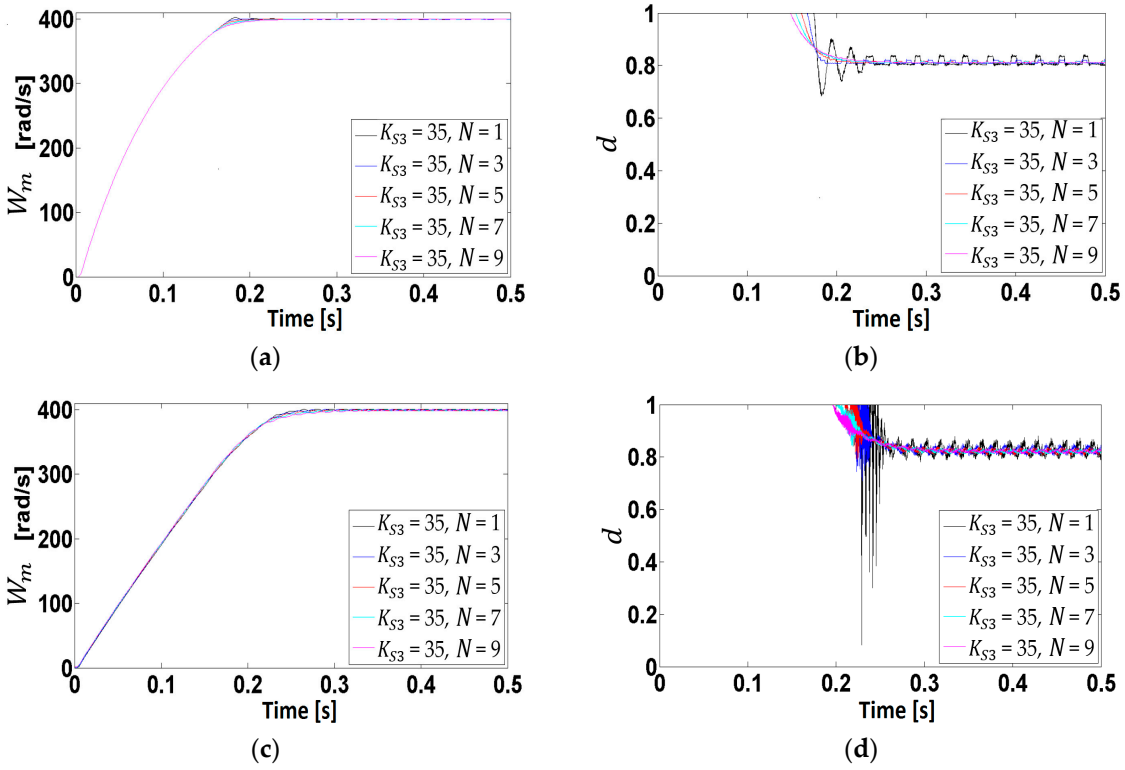

Figure 9. Behavior of the buck-motor system in closed-loop while changing N with $K_{S3} = 35$: (**a**) output W_m for the simulation; (**b**) d for the simulation; (**c**) output W_m for the experiment; and (**d**) d for the experiment.

Tables 5 and 6 summarize the results shown in Figure 9. Both the simulation and experimental test show that the steady-state error is less than 1% for the different values of the parameter N. If the value of N is increased or decreased, then it does not greatly affect the dynamics in the transient state. However, for small values of N, some small oscillations are presented and they will increase in amplitude if N is reduced below 1.

Table 5. Transient results obtained from the simulation in a closed loop with ZAD-FPIC.

Parameter	M_p (%)	t_s (s)	Error (%)
(N = 1)	0.5717	0.1701	−0.0173
(N = 3)	Overdamped	0.1701	−0.0173
(N = 5)	Overdamped	0.1711	−0.0173
(N = 7)	Overdamped	0.1737	−0.1473
(N = 9)	Overdamped	0.1802	−0.0173

Table 6. Transient results for the experimental test when the system works in closed loop with ZAD-FPIC.

Parameter	M_p (%)	t_s (s)	Error (%)
(N = 1)	Overdamped	0.2311	0.2775
(N = 3)	Overdamped	0.2381	0.2772
(N = 5)	Overdamped	0.2414	−0.3118
(N = 7)	Overdamped	0.2455	−0.3118
(N = 9)	Overdamped	0.2505	−0.4590

Because the model is not exact, for all values of N, the system responds faster in the simulation than in the experimental test. Regarding the duty cycle, Figure 9b,d show the saturation at the beginning; however, during the steady-state the duty cycle is not saturated for any value of N, which leads to a fixed commutation frequency that reduces the electrical and audible noises in the experimental test. Figure 9d shows electronic noise present in the measured signals. In general, for all values of N, the simulation and experimental tests show similar results.

3.4. Variation of the Parameter K_{S3}

Figures 10 and 11 show the bifurcation parameters of W_m and d for the experimental test when the parameter K_{S3} is changed. Figures 10 and 11–d show the behavior of W_m and d over time for the experimental test for $K_{S3} = 40$, $K_{S3} = 20$, and $K_{S3} = 5$, when the values of $K_{S1} = K_{S2} = 2$, and N = 1. The results show that for the value of $K_{S3} = 40$, some 4T periodic orbits are presented, which is the behavior clearly represented in Figure 10b. For the value of $K_{S3} = 20$, Figure 10a shows 6T periodic orbits, which can be represented in Figure 10c. For the value of $K_{S3} = 5$, Figure 10a shows 8T periodic orbits, which is easily represented as Figure 10d. For the duty cycle d in both diagrams, some chaotic and quasi-periodic behaviors are presented for different values of K_{S3} as shown in Figure 11.

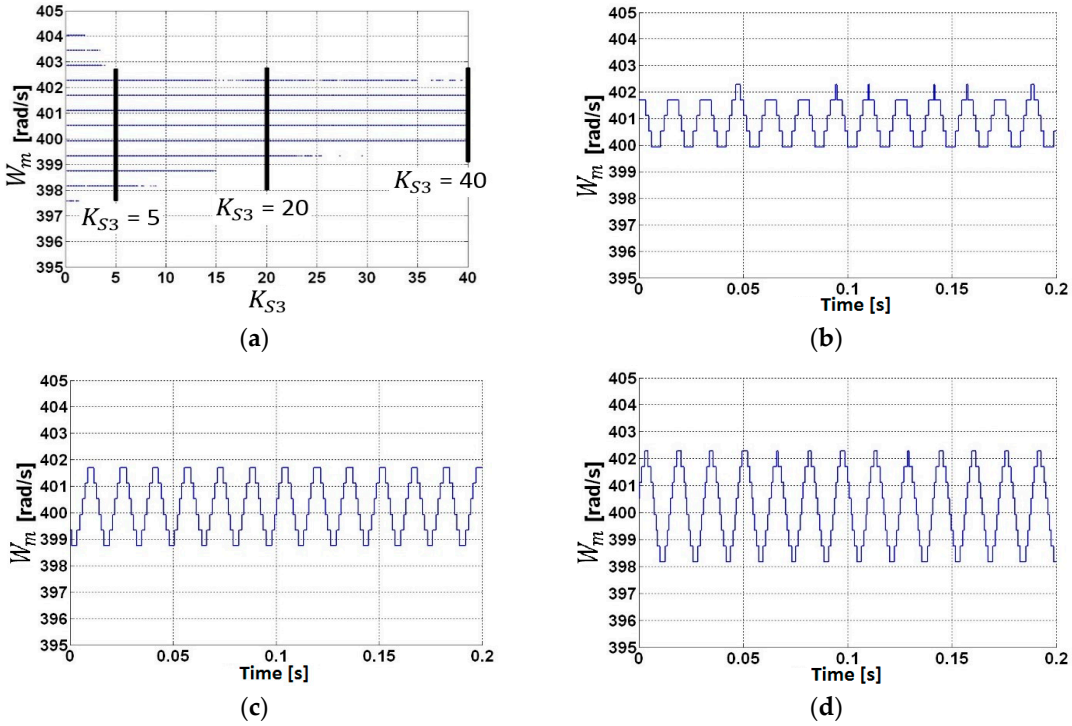

Figure 10. Bifurcation diagram of the variable W_m when the parameter K_{S3} is changed ($K_{S3} = 40$, $K_{S3} = 20$, and $K_{S3} = 5$) and the values of $K_{S1} = K_{S2} = 2$, and $N = 1$ are kept constant: (**a**) bifurcation diagram W_m vs. K_{S3} for the experimental test; (**b**) W_m in the experimental test when $K_{S3} = 40$; (**c**) W_m in the experimental test when $K_{S3} = 20$; and (**d**) W_m in the experimental test when $K_{S3} = 5$.

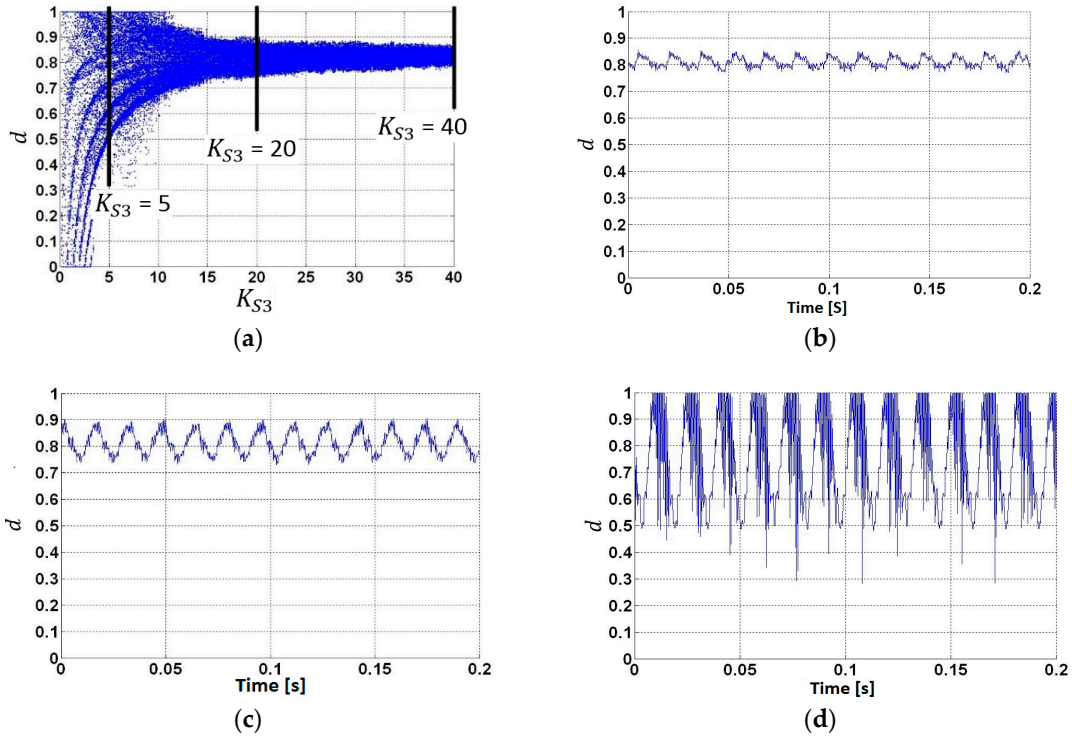

Figure 11. Bifurcation diagram of d vs. K_{S3} and behavior of $K_{S3} = 40$, $K_{S3} = 20$, and $K_{S3} = 5$ when the values of $K_{S1} = K_{S2} = 2$ and $N = 1$: (**a**) bifurcation diagram of d vs. K_{S3} in the experimental test; (**b**) behavior of d when $K_{S3} = 40$ in the experimental test; (**c**) behavior of d when $K_{S3} = 20$ in the experimental test; and (**d**) behavior of d when $K_{S3} = 5$ in the experimental test.

3.5. Behavior of the System When the Control Parameter N of the FPIC Is Changed

Figures 12 and 13 show the behavior of the buck-motor system controlled by ZAD when the parameter $K_{S3} = 35$ and the parameters K_{S1} and K_{S2} are equal to two. In this case, some bifurcations were created with the change of parameter N for the system with one delay period. The results show that the critical N in the simulation test was presented when $N \cong 0.7875$ and in the experimental test when $N \cong 0.5$. For values of N greater than the bifurcation point, the stability of the system was presented and the regulated variable (W_m) tends to the fixed point. Therefore, with values of $N = 1$ and $K_{S3} = 35$, there was good regulation as observed in Figure 12a,b. In the simulation test, with values of $N \leq 0.7875$, the system presents chaos and quasi-periodicity behaviors, whereas in the experimental test they occur for $N \leq 0.5$.

In the simulation test, stability was presented for values of $N \geq 0.7875$, whereas in the experimental test it was presented for values of $N \geq 0.5$. For these same values of N, a quasi-periodicity behavior occurs in the duty cycle, but a fixed switching frequency was achieved. Regarding the steady-state error, a value lower than 1% in the entire range of N was presented. In general, both the numerical and experimental diagrams were similar, thus validating the use of the model and the implemented circuit. Therefore, the ZAD-FPIC technique presented good performance to control the W_m and the FPIC technique demonstrated effectiveness to control chaos of the electric circuit.

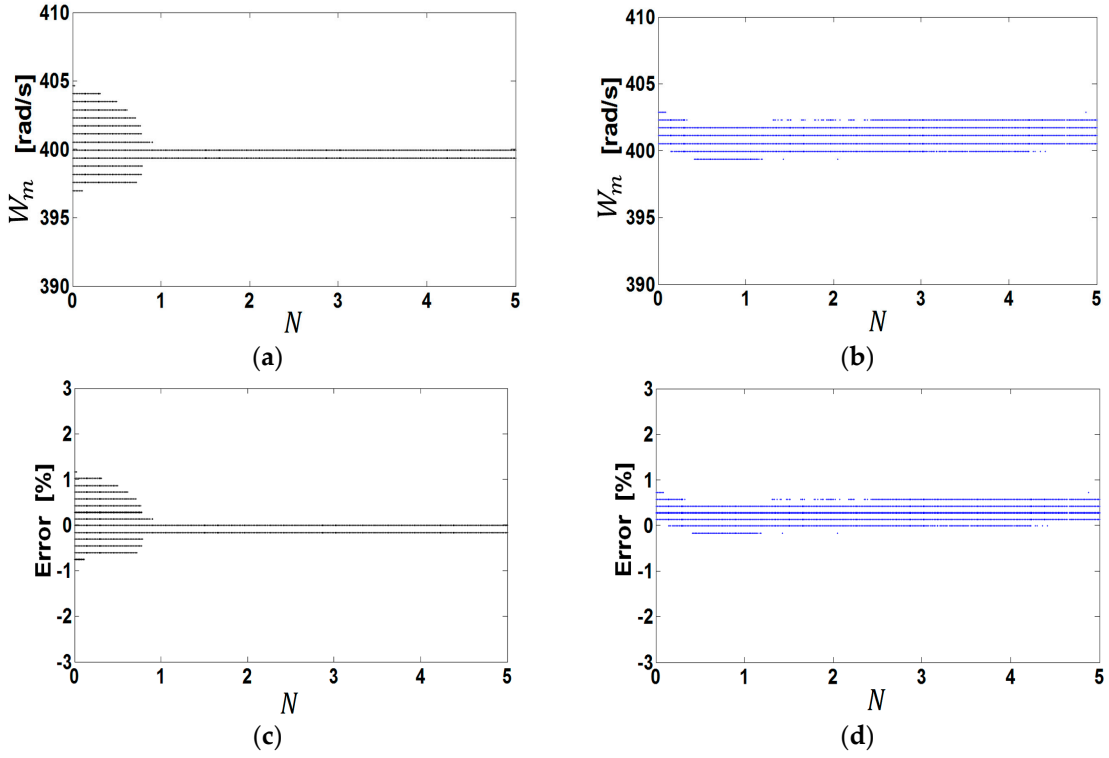

Figure 12. Bifurcation diagrams for the simulation and experimental test of the system with ZAD ($K_{S3} = 35$) and FPIC, changing the parameter N and maintaining fixed values of $K_{S1} = K_{S2} = 2$: (**a**) W_m vs. N for the simulation test; (**b**) W_m vs. N for the experimental test; (**c**) error vs. N for the simulation test; and (**d**) error vs. N for the experimental test.

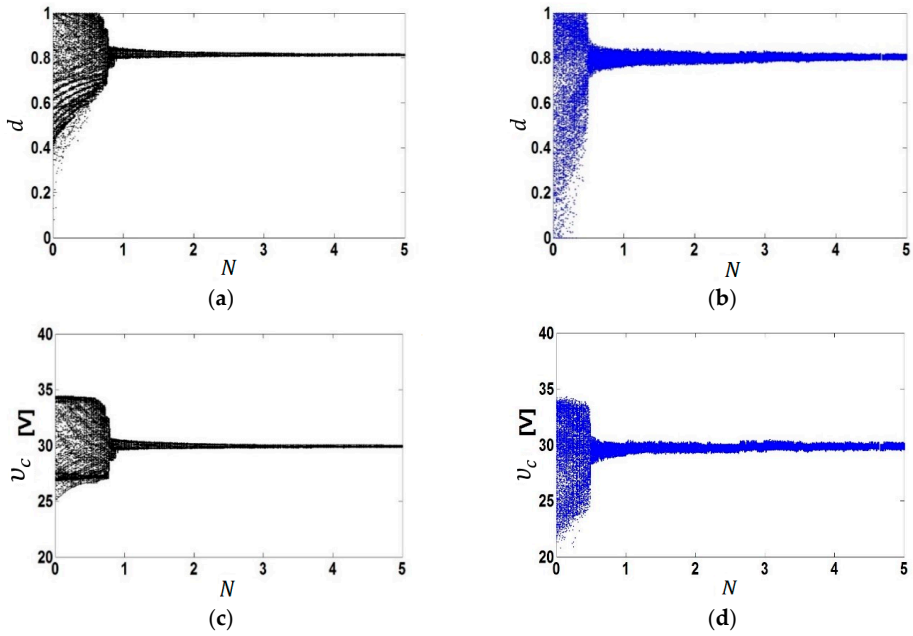

Figure 13. Bifurcation diagrams for the simulation and experimental test of the system with ZAD ($K_{S3} = 35$) and FPIC, changing the parameter N and maintaining fixed values of $K_{S1} = K_{S2} = 2$: (**a**) d vs. N for the simulation test; (**b**) d vs. N for the experimental test; (**c**) v_c vs. N for the simulation test; and (**d**) v_c vs. N for the experimental test.

Figures 14 and 15 show the behavior of the buck-motor system controlled with ZAD-FPIC with two delay periods. In this case, the equilibrium point has shifted slightly to the right when the critical N is approximately N = 2.2 in the experimental test and N = 2.24 in the simulation. Figures 14 and 15 show that the signals in both the numerical and experimental tests have similar behavior, validating that the circuits modeled and built for the tests are correct.

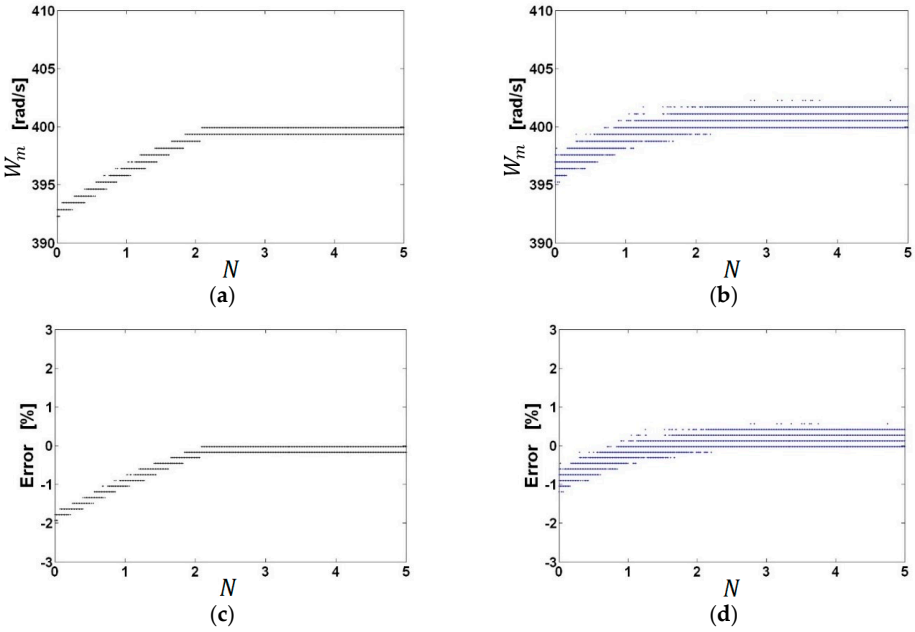

Figure 14. Bifurcation diagrams for the simulation and experimental test of the system with ZAD ($K_{S3} = 35$) and FPIC, changing the parameter N with $K_{S1} = K_{S2} = 2$ and a 2T delay period: (**a**) W_m vs. N for the simulation test; (**b**) W_m vs. N for the experimental test; (**c**) error vs. N for the simulation test; and (**d**) error vs. N for the experimental test.

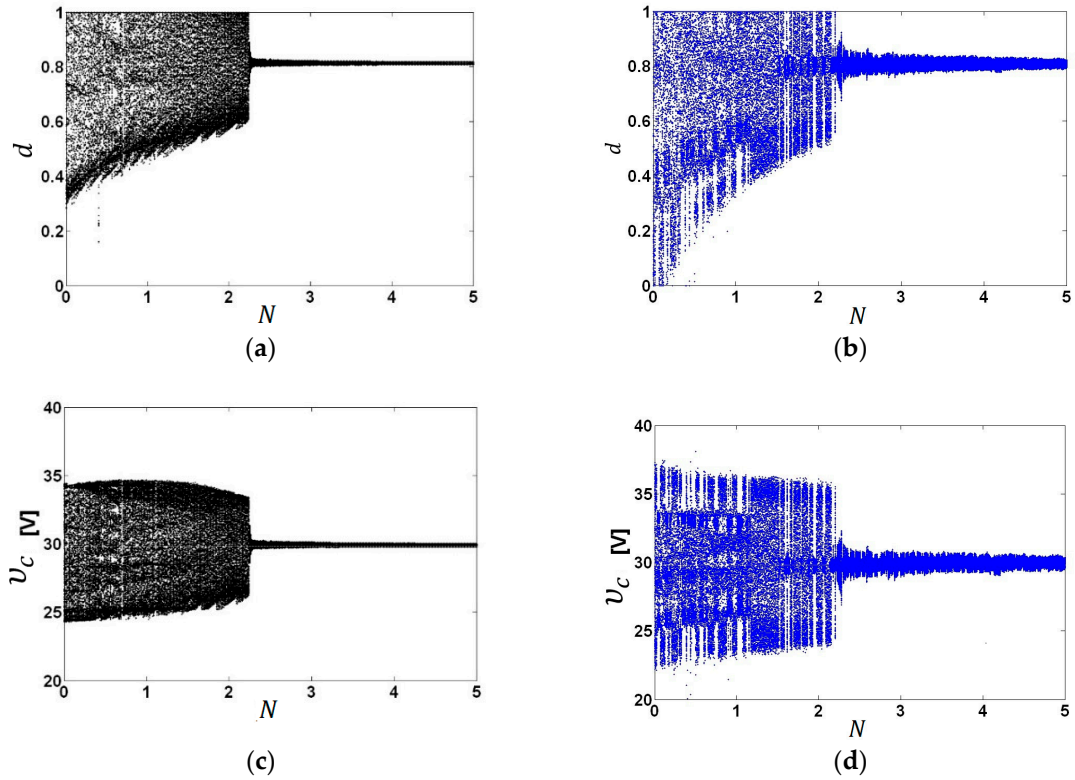

Figure 15. Bifurcation diagrams for the simulation and experimental test of the system with ZAD ($K_{S3} = 35$) and FPIC, changing the parameter N with $K_{S1} = K_{S2} = 2$ and a 2T delay period: (**a**) d vs. N for the simulation test; (**b**) d vs. N for the experimental test; (**c**) v_c vs. N for the simulation test; and (**d**) v_c vs. N for the experimental test.

3.6. Perturbation at the Input Voltage

This section shows the behavior of the system when V_{in} is changed. To carry out these experiments, the signal V_{in} was measured and registered with the DS1104MUXADC block, which was configured by the trigger signal at a frequency F_s. For these tests, the parameters of Table 3 were considered: $N = 1$, $K_{S1} = K_{S2} = 2$, and $K_{S3} = 35$.

Figure 16 shows the behavior of the buck-motor system described in Figure 2 and with the parameters of Table 3. Figure 16a shows the behavior of the system when instantaneous perturbations are created in V_{in} as performed for the experimental test. Figure 16b shows the effect in the regulated signal W_m by changing V_{in} and maintaining a value of W_m = 198 rad/s and reference signal W_{mref} = 200 rad/s. Figure 16c shows that the regulation error was maintained at the value of -1%. Figure 16d shows a phase diagram between the regulation error and V_{in} in which it is observed that the error was maintained at the value of -1%.

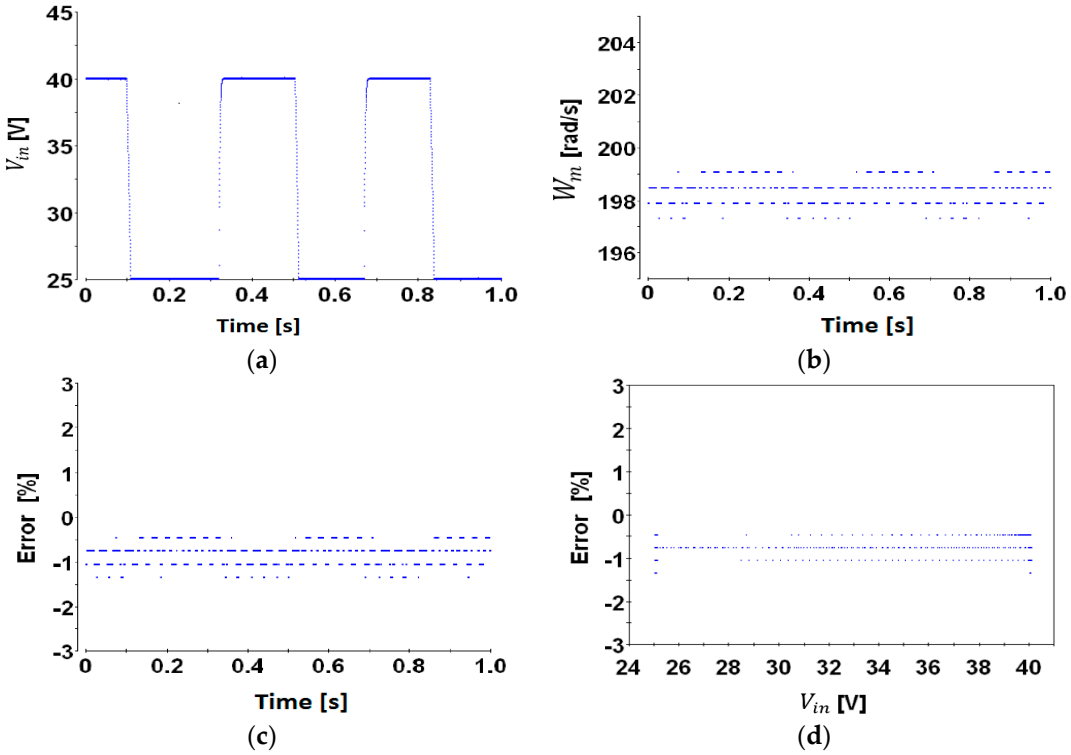

Figure 16. Behavior of the buck-motor system when perturbations in V_{in} are presented for the experimental test with $K_{S3} = 40$, $K_{S1} = K_{S2} = 2$, and $N = 1$: (**a**) variation of V_{in} over time; (**b**) regulated signal W_m over time; (**c**) error in the controlled variable; and (**d**) phase diagram of the error vs. V_{in}.

Figures 17 and 18 show the behavior of the regulation error in the experimental test when V_{in} was disturbed irregularly. In the first test, V_{in} was increased as shown in Figure 17a, and for this input, Figure 17b presents the results of the error vs. V_{in}, where the ZAD-FPIC controls the output signal with an error lower than -2%. For the second test, V_{in} was initially increased and then further decreased as shown in Figure 18a, and the error of the control variable vs. V_{in} does not exceed -2% as shown in Figure 18b.

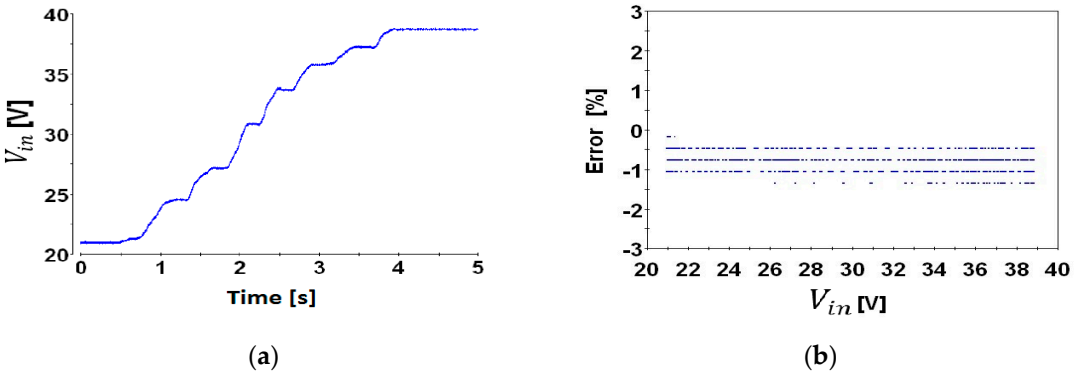

Figure 17. Experimental behavior of the buck-motor system after perturbations in V_{in} when $K_{S3} = 40$, $K_{S1} = K_{S2} = 2$, and $N = 1$: (**a**) variation in V_{in} over time and (**b**) phase diagram of error vs. V_{in}.

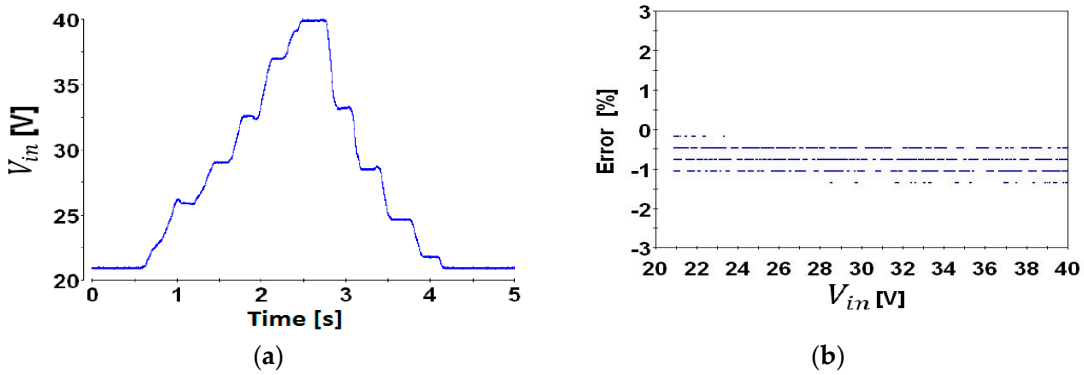

Figure 18. Experimental behavior of the buck-motor system after perturbations in V_{in} when $K_{S3} = 40$, $K_{S1} = K_{S2} = 2$, and $N = 1$: (**a**) variation of V_{in} over time and (**b**) phase diagram of the error vs. V_{in}.

4. Conclusions

This paper presented the dynamic behavior of a buck-motor system controlled with ZAD-FPIC. The results show that the control regulates very well the speed at the output W_m for different values of the reference signal (W_{mref}). When $K_{S3} = 35$ and increasing the value of $N > 1$, the dynamic response of the system was very similar for different values of N. The ZAD-FPIC control technique was effective to control the buck-motor system even for two delay periods and the robustness of the system was checked by making variations in V_{in}. When the control parameter of the ZAD was a fixed value and the FPIC control parameter changed, the transient behavior showed that neither the transient nor stationary regime changed with the change of N. Numerically and experimentally, orbits of periods $6T$, $8T$, and chaos were shown, which were plotted in the bifurcation diagrams against time. For the case where there were two periods of delay, the controller with ZAD-FPIC was able to regulate the output speed with low steady-state error.

Previous works have shown that the duty cycle is normally saturated and the electrical and audible noises increase. With the ZAD-FPIC control technique, greater stability and noise reduction were obtained in the controlled variable and in the voltage feeding the motor due to the fixed frequency switching implemented in the control technique. Some clear advantages of this controller were obtained when the control parameters had higher values because the system was more stable and did not present chaos; besides, the controller presented a low steady-state error in the controlled variable. However, when using the ZAD-FPIC control technique, the system became less robust to real-time variations of the system parameters because the duty cycle depended directly on these parameters. Furthermore, the controller depended on all the variables of the system, increasing the time for digital processing and real-time calculation of the duty cycle, requiring more powerful processors.

Author Contributions: F.E.H.V. conceived the theory, performed the experiments, and analyzed the data; J.E.C.-B. wrote the paper, reviewed the theory, performed simulations, and analyzed the data; A.R.S. helped with the design of the control and reviewed the theory.

Funding: This research received no external funding.

Acknowledgments: This work was supported by the Universidad Nacional de Colombia, Sede Manizales and Sede Medellín under the projects HERMES-34671 and HERMES-36911. The authors thank the School of Physics and the Department of Electrical Energy and Automation for their valuable support to conduct this research.

Conflicts of Interest: The authors declare no conflict of interest.

References

1. Cuong, N.D.; Van Lanh, N.; Dinh, G.T. An Adaptive LQG Combined With the MRAS—Based LFFC for Motion Control Systems. *J. Autom. Control Eng.* **2015**, *3*, 130–136. [CrossRef]
2. Sankardoss, V.; Geethanjali, P. PMDC Motor Parameter Estimation Using Bio-Inspired Optimization Algorithms. *IEEE Access* **2017**, *5*, 11244–11254. [CrossRef]

3. Hilairet, M.; Auger, F. Speed sensorless control of a DC-motor via adaptive filters. *IET Electr. Power Appl.* **2007**, *1*, 601. [CrossRef]
4. Hu, H.; Yousefzadeh, V.; Maksimovic, D. Nonuniform A/D Quantization for Improved Dynamic Responses of Digitally Controlled DC-DC Converters. *IEEE Trans. Power Electron.* **2008**, *23*, 1998–2005. [CrossRef]
5. Fung, C.W.; Liu, C.P.; Pong, M.H. A Diagrammatic Approach to Search for Minimum Sampling Frequency and Quantization Resolution for Digital Control of Power Converters. In Proceedings of the 2007 IEEE Power Electronics Specialists Conference, Orlando, FL, USA, 17–21 June 2007; pp. 826–832.
6. Taborda, J.A.; Angulo, F.; Olivar, G. Estimation of parameters in Buck converter with Digital-PWM control based on ZAD strategy. In Proceedings of the 2011 IEEE Second Latin American Symposium on Circuits and Systems (LASCAS), Bogota, Colombia, 23–25 February 2011; pp. 1–4.
7. Zane, M. Erickson Impact of digital control in power electronics. In Proceedings of the 16th International Symposium on Power Semiconductor Devices & IC's, Kawasaki, Japan, 24–27 May 2004; pp. 13–22.
8. Hoyos, F.E.; Rincón, A.; Taborda, J.A.; Toro, N.; Angulo, F. Adaptive Quasi-Sliding Mode Control for Permanent Magnet DC Motor. *Math. Probl. Eng.* **2013**, *2013*, 693685. [CrossRef]
9. Fossas, E.; Griñó, R.; Biel, D. Quasi-Sliding control based on pulse width modulation, zero averaged dynamics and the L2 norm. In *Advances in Variable Structure Systems, Proceedings of the 6th IEEE International Workshop on Variable Structure Systems, Coolangatta, Australia, 7–9 December 2000*; World Scientific: Singapore, 2000; pp. 335–344.
10. Biel, D.; Fossas, E.; Ramos, R.; Sudria, A. Programmable logic device applied to the quasi-sliding control implementation based on zero averaged dynamics. In Proceedings of the 40th IEEE Conference on Decision and Control (Cat. No.01CH37228), Orlando, FL, USA, 4–7 December 2001; Volume 2, pp. 1825–1830.
11. Ramos, R.R.; Biel, D.; Fossas, E.; Guinjoan, F. A fixed-frequency quasi-sliding control algorithm: Application to power inverters design by means of FPGA implementation. *IEEE Trans. Power Electron.* **2003**, *18*, 344–355. [CrossRef]
12. Angulo, F.; Fossas, E.; Olivar, G. Transition from Periodicity to Chaos in a PWM-Controlled Buck Converter with ZAD Strategy. *Int. J. Bifurc. Chaos* **2005**, *15*, 3245–3264. [CrossRef]
13. Angulo, F.; Olivar, G.; di Bernardo, M. Two-parameter discontinuity-induced bifurcation curves in a ZAD-strategy-controlled dc-dc buck converter. *IEEE Trans. Circuits Syst. I Regul. Pap.* **2008**, *55*, 2392–2401. [CrossRef]
14. Fossas, E.; Hogan, S.J.; Seara, T.M. Two-parameter bifurcation curves in power electronics converters. *Int. J. Bifurc. Chaos* **2009**, *19*, 349–357. [CrossRef]
15. Hoyos, F.E.; Candelo-Becerra, J.E.; Toro, N. Numerical and experimental validation with bifurcation diagrams for a controlled DC–DC converter with quasi-sliding control. *TecnoLógicas* **2018**, *21*, 147–167. [CrossRef]
16. Di Bernardo, M.; Budd, C.; Champneys, A. Grazing, skipping and sliding: Analysis of the non-smooth dynamics of the DC/DC buck converter. *Nonlinearity* **1998**, *11*, 859–890. [CrossRef]
17. Yuan, G.; Banerjee, S.; Ott, E.; Yorke, J.A. Border-collision bifurcations in the buck converter. *IEEE Trans. Circuits Syst. I Fundam. Theory Appl.* **1998**, *45*, 707–716. [CrossRef]
18. Hoyos, F.E.; Candelo, J.E.; Silva-Ortega, J.I. Performance evaluation of a DC-AC inverter controlled with ZAD-FPIC. *Inge CUC* **2018**, *14*, 9–18. [CrossRef]
19. Biel, D.; Cardoner, R.; Fossas, E. Tracking Signal in a Centered Pulse ZAD Power Inverter. In Proceedings of the International Workshop on Variable Structure Systems, Sardinia, Italy, 5–7 June 2006; pp. 104–109.
20. Biel, D.; Fossas, E.; Guinjoan, F.; Ramos, R. Interleaving quasi-sliding mode control of parallel-connected inverters. In Proceedings of the 2008 International Workshop on Variable Structure Systems, Antalya, Turkey, 8–10 June 2008; pp. 337–342.
21. Angulo, F.; Olivar, G.; Taborda, J.; Hoyos, F. Nonsmooth dynamics and FPIC chaos control in a DC-DC ZAD-strategy power converter. In Proceedings of the ENOC, EUROMECH Nonlinear Dynamics Conference, Saint Petersburg, Russia, 6–10 July 2008; pp. 1–6.
22. Rincón, A.; Hoyos, F.E.; Angulo, F. Controller Design for a Second-Order Plant with Uncertain Parameters and Disturbance: Application to a DC Motor. *Abstr. Appl. Anal.* **2013**, *2013*, 169519. [CrossRef]

23. Hoyos, F.E.; Candelo, J.E.; Taborda, J.A. Selection and validation of mathematical models of power converters using rapid modeling and control prototyping methods. *Int. J. Electr. Comput. Eng.* **2018**, *8*, 1551. [CrossRef]
24. Hoyos, F.E.; Burbano, D.; Angulo, F.; Olivar, G.; Toro, N.; Taborda, J.A. Effects of Quantization, Delay and Internal Resistances in Digitally ZAD-Controlled Buck Converter. *Int. J. Bifurc. Chaos* **2012**, *22*, 1250245. [CrossRef]